



Article

Damage Model of Carbon-Fiber-Reinforced Concrete Based on Energy Conversion Principle

Ruiqi Zheng *, Jianyong Pang *, Jian Sun, Yongqiang Su and Guoping Xu

School of Civil Engineering and Architecture, Anhui University of Science and Technology, Huainan 232001, China; 2021200328@aust.edu.cn (J.S.)

* Correspondence: 2021200346@aust.edu.cn (R.Z.); jypang@aust.edu.cn (J.P.)

Abstract: In order to enhance the practical application of carbon-fiber-reinforced concrete (CFRC) in engineering, it is necessary to study the damage mechanism of CFRC. Experimental research on the mechanical properties of CFRC under multiple strain rates was conducted. Five different fiber contents were analyzed to study the compressive strength and tensile strength of CFRC, and the damage characteristics of CFRC under multiple strain rates were analyzed based on failure modes and energy changes. An energy-based damage constitutive model was established. The results showed the following: (1) When the carbon fiber content was 0.4%, CFRC had the best comprehensive performance, with a 15.02% increase in compressive strength and a 51.12% increase in tensile strength. With the increase in strain rate, the compressive strength of the concrete increased. (2) Under high strain rates, carbon fiber significantly enhanced the compressive strength of the concrete, and the input energy, elastic strain energy, and dissipated energy increased. The peak value of the elastic strain energy conversion rate increased, and the minimum value of the dissipated energy conversion rate decreased. (3) Under the same strain rate, the CFRC had a larger inflection point of dissipated energy corresponding to the strain compared to the reference group of concrete during the loading process. A constitutive model for CFRC was established based on damage mechanics and probability statistics. The research results will provide theoretical references for the application of carbon-fiber-reinforced concrete.

Keywords: concrete; carbon fiber; damaged model; energy; mechanical properties; strain rate



Citation: Zheng, R.; Pang, J.; Sun, J.; Su, Y.; Xu, G. Damage Model of Carbon-Fiber-Reinforced Concrete Based on Energy Conversion Principle. *J. Compos. Sci.* **2024**, *8*, 71. <https://doi.org/10.3390/jcs8020071>

Academic Editor: Jiadeng Zhu

Received: 10 January 2024

Revised: 29 January 2024

Accepted: 7 February 2024

Published: 10 February 2024



Copyright: © 2024 by the authors. Licensee MDPI, Basel, Switzerland. This article is an open access article distributed under the terms and conditions of the Creative Commons Attribution (CC BY) license (<https://creativecommons.org/licenses/by/4.0/>).

1. Introduction

Building materials are one of the key factors affecting the performance of building structures [1]. Concrete is a porous brittle material commonly used in civil engineering [2]. Its failure characteristics include quasibrittle failure; that is, once failure occurs, the load-bearing capacity is almost completely lost [3]. To ensure the safety and durability of the project, modified concrete [4] was developed. Incorporating fibers into concrete for modification can play a role in reinforcement, crack resistance, and impermeability [5–8]. Among them, carbon fiber has attracted great attention due to its excellent properties such as its high specific modulus and high specific strength [9].

Existing studies have shown that carbon fibers can significantly improve the mechanical properties and durability of concrete materials [10–13]. Studies by Kizilkanat [14] have shown that the overall performance of CFRC is best when the carbon fiber content is 0.5%. To improve the frost resistance of concrete, Kan et al. [15] added carbon fibers to the concrete. The results show that the addition of carbon fibers in concrete can reduce the mass loss of concrete in freeze–thaw experiments. These studies have shown that the research content of CFRC has engineering significance. However, most of these studies only focused on the effect of carbon fiber content on the static loading properties of CFRC. We need to further explore the damage mechanism of CFRC. Deng et al. [16] studied the mechanical properties of carbon-fiber-reinforced coral aggregate concrete and proposed

that the damage model can effectively reflect the stress–strain relationship of FRCAC. However, the damage to concrete specimens is closely related to energy dissipation, and the constitutive model parameters do not involve energy. The energy method is commonly used to represent the damage and failure characteristics of concrete materials when studying the properties of concrete materials under dynamic loads [17–19]. Based on the principle of energy dissipation, Li et al. [20] established the relationship between the energy consumption density and the fractal dimension of concrete under dynamic loading and revealed the characteristics of the microdamage and macrofracture of concrete and the law of energy dissipation. Therefore, we can try to use energy methods to study the damage mechanism of CFRC under static load.

To sum up, there has been a lot of research on concrete materials, but most of it focuses on the mechanical properties of concrete materials, and there are fewer studies based on the energy characteristics and damage constitutive models of carbon-fiber-reinforced concrete. In order to make carbon-fiber-reinforced concrete widely used in practical engineering, it is necessary to study the damage mechanism of carbon-fiber-reinforced concrete. CFRC with five kinds of fiber content (0%, 0.2%, 0.4%, 0.6%, and 0.8%) was prepared in this paper. The uniaxial compression test of CFRC under a multistrain rate was carried out to study the influence of different carbon fiber contents and different strain rates on the mechanical properties of CFRC. Based on the principle of energy conversion, combined with the failure mode of CFRC, the failure characteristics of CFRC under a multistrain rate are analyzed. Based on the principle of energy conversion, the damage model of carbon fiber concrete is proposed. The specific study process of this paper is shown in Figure 1.

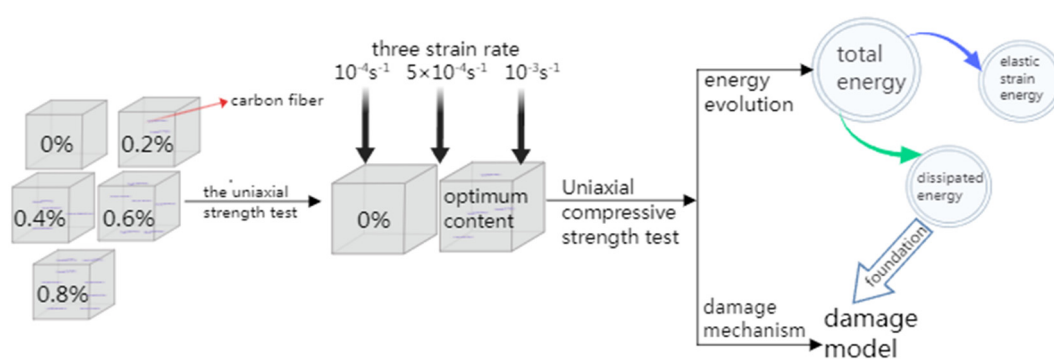


Figure 1. Study process.

2. Test Materials and Methods

2.1. Materials

The cement used is ordinary Portland cement of grade P.O. 42.5. The density of the cement is $2900 \text{ kg}\cdot\text{m}^{-3}$. The carbon fiber is straight. The main performance parameters are listed in Table 1. The sand used in the test is ordinary Huaihe River sand with a silicon content of 97.89%, an apparent density of $2510 \text{ kg}\cdot\text{m}^{-3}$, and a fineness modulus of 2.67. The apparent density of the coarse aggregate is $2609 \text{ kg}\cdot\text{m}^{-3}$, the particle size is 5~31.5 mm continuously graded gravel, the bulk density is $1575 \text{ kg}\cdot\text{m}^{-3}$, and the mud content is 1.1%. Water is normal tap water. The water-reducing agent is a PCA-I type superplasticizer, and the water reduction rate is 30%.

Table 1. Key performance parameters of carbon fiber.

Density /($\text{kg}\cdot\text{m}^{-3}$)	Tensile Strength/MPa	Length /mm	Carbon Content/%	Diameter / μm	Tensile Modulus/GPa
1800	3450	3	95	7	230

2.2. Experimental Design

In this experiment, there are five groups with different mixing ratios, where the carbon fiber content is 0, 0.2%, 0.4%, 0.6%, and 0.8%, marked as C₀, C_{0.2}, C_{0.4}, C_{0.6}, and C_{0.8} respectively. Specific mixing ratios are listed in Table 2.

Table 2. Mixing ratio of carbon fiber concrete specimens (kg·m⁻³).

Specimens	Cement	Fine Aggregate	Coarse Aggregate	Water	Carbon Fiber
C ₀	361	650	1360	145	0
C _{0.2}	361	650	1360	145	3.6
C _{0.4}	361	650	1360	145	7.2
C _{0.6}	361	650	1360	145	10.8
C _{0.8}	361	650	1360	145	14.4

Nine 100 mm × 100 mm × 100 mm cube specimens were prepared for the cube compressive strength test of each group, and three 100 mm × 100 mm × 100 mm cube specimens were prepared for the tensile strength test of each group.

In this study, a WAW-1000 electrohydraulic servo universal testing machine was used, and the main parameters are shown in Table 3. The experimental process was operated according to the requirements of GB/T 50081-2002 [21]. First, the uniaxial strength test of the cube specimen was carried out, and the test results were analyzed to determine the optimal carbon fiber content. Then, the optimal content group and the reference group were subjected to compressive strength tests at different strain rates (10⁻⁴s⁻¹, 5 × 10⁻⁴s⁻¹, and 10⁻³s⁻¹).

Table 3. Main technical parameters of electrohydraulic servo uniaxial testing machine.

Subject	Parameter
Maximum axial test force	3000 kN
Test force accuracy	±1%
Displacement range	100 mm
Displacement accuracy	±2%
Displacement equal velocity control	0.5~50 mm/min
Power supply	4 kW/AC380V/50 Hz

2.3. Specimen Making

Add cement, gravel, and sand to the blender in turn and stir for 3 min. Then, add a small amount of fiber to the blender many times, stir the fiber completely, and then stir the superplasticizer and water evenly into the blender for 4 min. After that, it is placed in a 100 mm × 100 mm × 100 mm cube mold with prelubricated oil. Finally, put it on the shaking table to vibrate the compaction molding. The molded concrete specimen was covered with plastic film for 24 h, and then the specimen was taken out for standard curing for 28 days.

2.4. Energy Calculation Method

Essentially, the failure process of materials is an energy-driven state instability phenomenon [22]. Therefore, it is of great importance to study the energy evolution of the uniaxial compressive failure of carbon fiber concrete to investigate the failure mechanism of carbon fiber concrete. According to the first law of thermodynamics, the energy conversion of carbon-fiber-reinforced concrete under uniaxial compression [23,24] can be expressed as follows:

$$U = U^e + U^d \tag{1}$$

where U is the total strain energy input per unit of working volume; U^e is the releasable elastic strain energy stored in the unit volume; and U^d is the energy dissipated per unit volume.

Figure 2 shows the relationship between U^e , U^d , and E_u in the stress failure process of CFRC specimens. The calculation of each energy can be expressed as follows:

$$U = \int_0^\epsilon \sigma d\epsilon \tag{2}$$

$$U^e = \frac{1}{2} \sigma \epsilon^e = \frac{1}{2E_u} \sigma^2 \tag{3}$$

$$U^d = U - U^e \tag{4}$$

where ϵ is the strain value of the specimen at a certain time; σ is the stress value of the specimen at a certain time, and the unit is MPa; and E_u is the elastic modulus of the specimen.

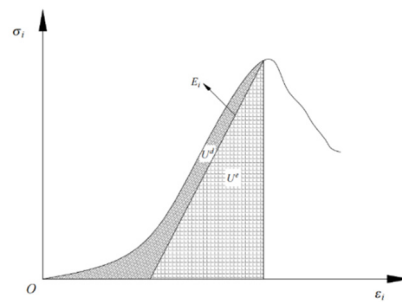


Figure 2. Energy distribution of carbon fiber concrete during uniaxial compression.

3. Compressive Test Results with Different CF Contents

3.1. Uniaxial Compressive Strength, Splitting Tensile Strength

The test results of concrete strength with different carbon fiber content are shown in Table 4. Compared to the plain concrete, the compressive strength remains on an upward trend with a carbon fiber content of 0–0.4%, but the increase is small. After that, with the increase in the carbon fiber content, the compressive strength began to decrease and was lower than the strength of the plain concrete, and the rate of decline was higher. At a carbon fiber content of 0.2%, 0.4%, 0.6%, and 0.8%, the compressive strength of the specimen is 4.93%, 15.02%, –15.02%, and –23.74% higher than that of the reference, respectively. The split tensile strength initially increases and then decreases with increasing carbon fiber content, and the overall tensile strength is higher than that of the reference group. At a carbon fiber content of 0.2%, 0.4%, 0.6%, and 0.8%, the tensile strength of the specimen is 41.32%, 51.12%, 46.26%, and 25.42% higher than that of the concrete of the reference group, respectively. This is because, with the appropriate amount of carbon fibers, the carbon fibers can be fully stirred and evenly distributed, creating a staggered network of fibers within the specimen, which acts as a bridge and stress transfer, preventing the aggregate from sinking into the specimen. The carbon fiber has excellent tensile properties. If the carbon fiber content is too high, agglomeration is easy to occur due to the poor distribution of carbon fibers, resulting in the deterioration of concrete workability and negative effects on the mechanical properties of concrete.

Table 4. Uniaxial compressive strength and splitting tensile strength of concrete specimens.

Specimens	C ₀	C _{0.2}	C _{0.4}	C _{0.6}	C _{0.8}
Compressive strength/MPa	43.456	45.6	49.982	36.928	33.14
Tensile strength/MPa	4.349	6.146	6.572	6.361	5.454

3.2. Stress–Strain Relationship

The stress–strain curve of concrete with different carbon fiber contents is shown in Figure 3. The failure process of concrete with different carbon fiber contents went through the compaction phase, the elastic deformation phase, the plastic deformation phase, and the failure phase. At the initial stage of loading, the internal pores of the specimen are compacted, and the stress–strain curves of the concrete specimen with different carbon fiber contents are concave. As the stress increases, the specimen enters the stage of elastic deformation, and the stress–strain curve is approximately linear. Under sustained loading, the specimen begins to show plastic deformation and enters the plastic deformation stage. As the load increases, the load reaches the maximum load capacity of the specimen. At the failure stage, the specimen begins to fail and the load capacity decreases.

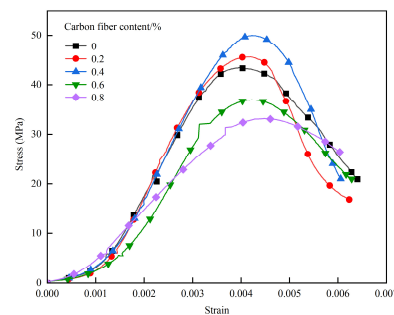


Figure 3. Stress–strain curves of concrete with different carbon fiber content.

Based on the above study, the compressive strength of CFRC (f) is as follows: $f_{0.4} > f_{0.2} > f_0 > f_{0.6} > f_{0.8}$; the tensile strength (R_m) is expressed as $R_{m0.4} > R_{m0.6} > R_{m0.2} > R_{m0.8} > R_{m0}$, and the peak strain (ϵ) is expressed as $\epsilon_{0.8} > \epsilon_{0.4} > \epsilon_{0.6} > \epsilon_{0.2} > \epsilon_0$.

3.3. Normal Strain Rate Failure Mode

Figure 4 shows the ultimate failure mode of the concrete specimens with different carbon fiber contents in compression tests. The failure of the reference concrete is brittle failure, the failure is more thorough, and the final failure mode is an hourglass type. As the fiber content increases, during the compression process, the surface spalling of the specimen becomes less. After loading, the integrity of the concrete specimen becomes higher and the overall failure mode is “cracks but not scattered”, which is different from the large-scale complete spalling of the specimen after the loss of the bearing capacity.

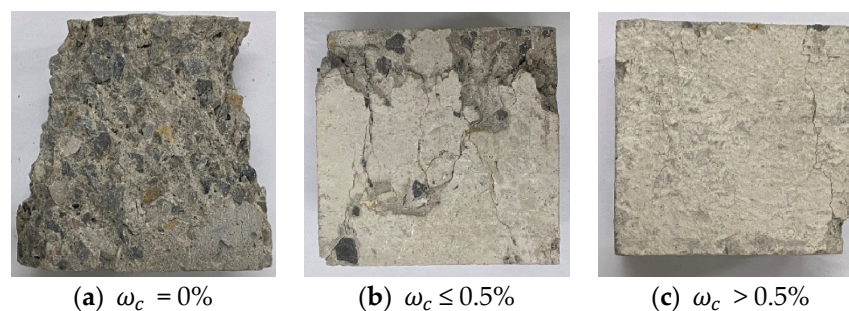


Figure 4. Failure modes of cube test blocks made of reference group concrete and carbon fiber concrete in compression tests.

Figure 5 shows the final failure mode of the tensile splitting test on the concrete specimens with different carbon fiber contents. The fracture surface of the concrete specimen of the reference group is complete under the splitting action, and the fracture surface is mainly of I type, which is close to the ideal splitting model of concrete [25]. When the fiber volume fraction is low, the fracture surface is dominated by two cracks (main cracks

and branch cracks), and the integrity of the fracture surface is not as good as that of the reference group concrete. When the fiber volume fraction is high, three obvious cracks appear on the fracture surface of the specimen, and the integrity of the fracture surface is poor.

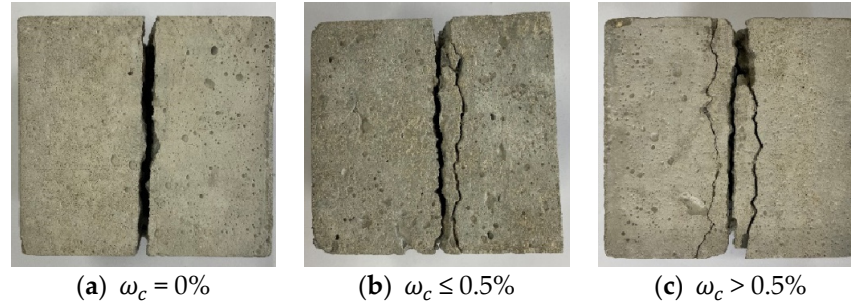


Figure 5. Failure patterns of cube test blocks made of reference group concrete and carbon fiber concrete in the split tensile test.

3.4. Energy Characteristics at Peak Load

The variation trend of the energy properties of the concrete specimens with different carbon fiber contents at peak stress is shown in Figure 6. The change trend of the input energy, elastic strain energy, and dissipation energy of the concrete specimens with different carbon fiber contents at peak stress is basically the same. When the carbon fiber content is less than or equal to 0.4%, the input energy and elastic strain energy of the carbon fiber concrete specimen at peak stress increase with an increase in the carbon fiber content. When the carbon fiber content is more than 0.4%, the input energy and elastic strain energy of the carbon fiber concrete specimen at the peak stress decrease with increasing carbon fiber content.

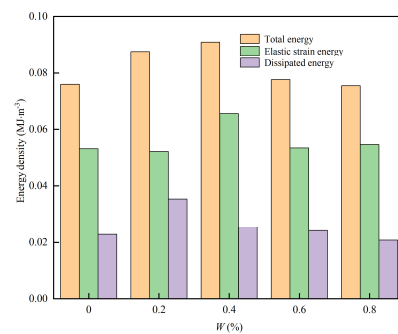


Figure 6. Energy properties of soil specimens at peak strain with different carbon fiber contents.

When the carbon fiber content is 0.4%, the input energy and elastic strain energy peak at the peak stress. The dissipated energy initially increases and then decreases as the carbon fiber content increases, and the dissipated energy at the peak voltage peaks when the carbon fiber content is 0.2%.

The compressive strength, peak strain, tensile strength, input energy, elastic strain energy, and dissipation energy at the peak strain of the concrete specimens with different carbon fiber contents were compared. The overall performance of the carbon fiber concrete was best at a carbon fiber content of 0.4%.

4. Compressive Test Results at Multiple Strain Rates

Uniaxial compression tests were carried out on the concrete of the reference group and concrete with 0.4% carbon fiber at different strain rates.

4.1. Uniaxial Compressive Strength

Figure 7 is the compressive strength histogram of the reference group concrete and 0.4% CFRC at different strain rates. At a strain rate of 10^{-4}s^{-1} , $5 \times 10^{-4}\text{s}^{-1}$, and 10^{-3}s^{-1} , the compressive strength of the 0.4% CFRC increases by 10.01%, 15.02%, and 18.27%, respectively, compared to the reference group concrete.

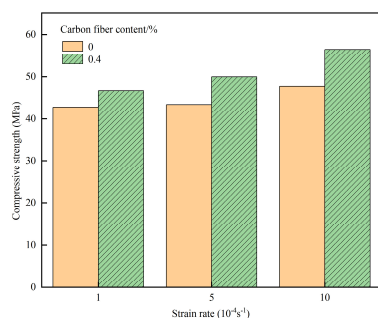


Figure 7. Compressive strength of C0 and C0.4 at different strain rates.

The compressive strength of the concrete specimens of the reference group and the 0.4% CFRC specimens increases with an increasing strain rate. With the increase in the strain rate, the compressive strength of the concrete in the reference group increased by 2.29% and 12.41%. The compressive strength of the 0.4% CFRC specimens increased by 6.95% and 20.85%. This is because the greater the strain rate, the shorter the time required to respond to the stretch and the greater the stress required for the stretch to occur. At the same strain rate, the compressive strength of the reference group concrete is lower than that of the 0.4% carbon fiber concrete, and at a high strain rate, carbon fiber can significantly improve the compressive strength of concrete.

4.2. Multi-Strain Rate Failure Modes

Figure 8 shows the failure modes of the concrete specimens at different strain rates. As the strain rate increases, the brittleness of the specimen increases and the integrity of the failure mode deteriorates. At a low strain rate, there are only cracks on the surface of the specimen, no obvious deposits and spalling, and the cracks are shallow. Under the high strain rate, when the specimen is destroyed, it is accompanied by a bursting sound, the surface of the specimen peels off obviously, and the surface crack deepens.

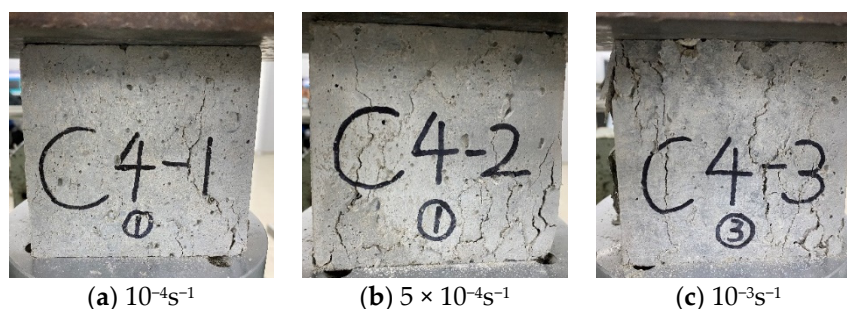


Figure 8. Failure patterns of concrete test blocks at different strain rates.

This is due to the fact that under higher strain rate conditions, the applied energy is absorbed by the initial cracks on the specimen surface and there is more form. These microcracks cause the specimen to break down into smaller fragments, which is different from the damage morphology of the quasistatic state. The compression testing of specimens under high strain rate conditions is characterized by impact damage to some extent [26].

4.3. Energy Development Laws and Transformation Properties

Figure 9 shows the energy development of concrete from the plain concrete and 0.4% CFRC at different strain rates (10^{-4}s^{-1} , $5 \times 10^{-4}\text{s}^{-1}$, and 10^{-3}s^{-1}). With the increase in the loading stress, the total energy, elastic strain energy, and dissipation energy of the CFRC and reference concrete are on the rise. When the stress increases to the peak stress, the total energy, elastic strain energy, and dissipation energy of the CFRC increase by 18.28%, 18.52%, and 17.70%, respectively, compared with the reference concrete at a 10^{-4}s^{-1} strain rate. At the strain rate of $5 \times 10^{-4}\text{s}^{-1}$, the total energy, elastic strain energy, and dissipated energy of the CFRC increased by 19.73%, 23.04%, and 12.01%, respectively. At the 10^{-3}s^{-1} strain rate, the total energy, elastic strain energy, and dissipation energy of the CFRC increased by 7.44%, 45.82%, and -43.32% , respectively. It can be found that the dissipation energy of the CFRC decreases at the 10^{-3}s^{-1} strain rate, but it can be clearly seen from Figure 9 that the corresponding peak strain increases compared with the reference concrete, which indicates that the effect of the fiber on improving the toughness of the concrete matrix is weakened at this strain rate.

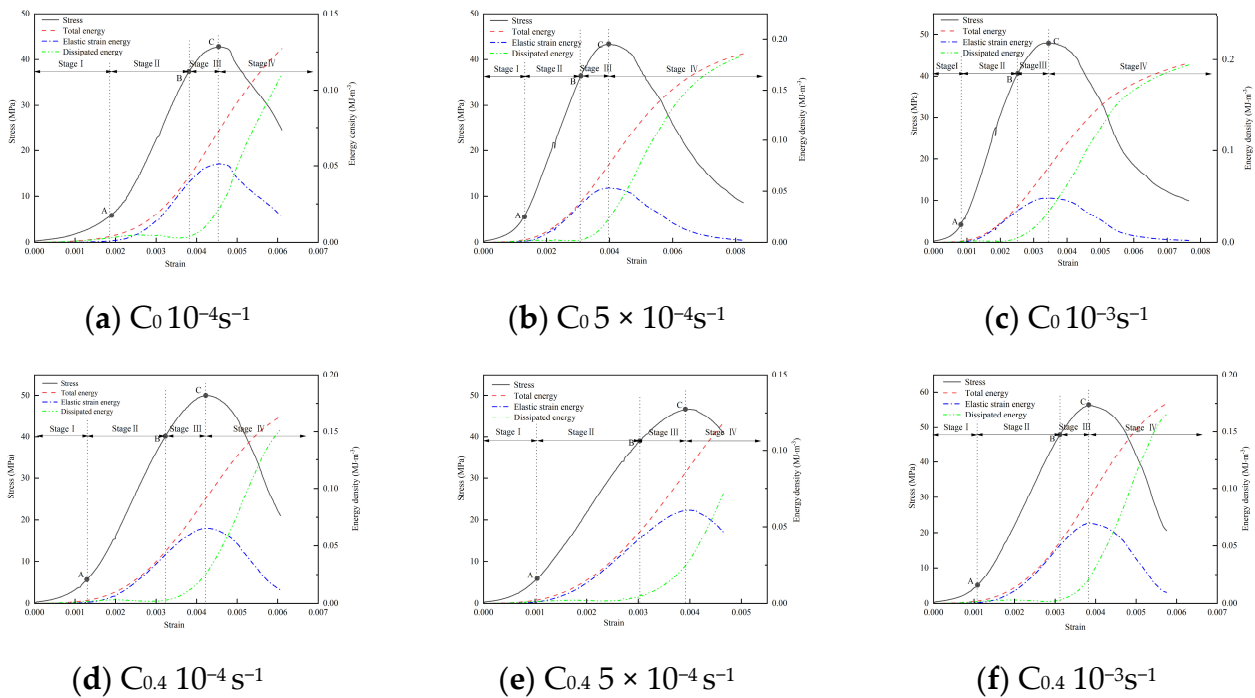


Figure 9. Energy evolution characteristics.

The destruction of the concrete specimens can be divided into four stages: the compaction stage (I), elastic deformation stage (II), plastic deformation stage (III), and destruction stage (IV). To express the energy conversion relationship intuitively, the energy conversion rate of elastic strain $\alpha = U_e/U$ and the energy conversion rate of dissipation $\beta = U_d/U$ are introduced. Using the example of the 0.4% CFRC at a strain rate of $5 \times 10^{-4}\text{s}^{-1}$, the relationship between the stress–strain curve and the energy conversion rate is shown in Figure 10. Figure 11a–c shows the strain rate of 10^{-4}s^{-1} , $5 \times 10^{-4}\text{s}^{-1}$, and 10^{-3}s^{-1} ; the reference group concrete; and a comparison table of the energy conversion rates of the concrete specimens with the 0.4% carbon fiber concrete.

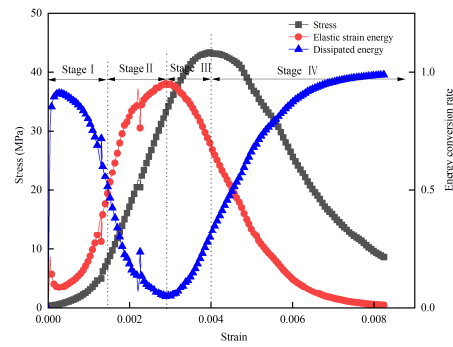
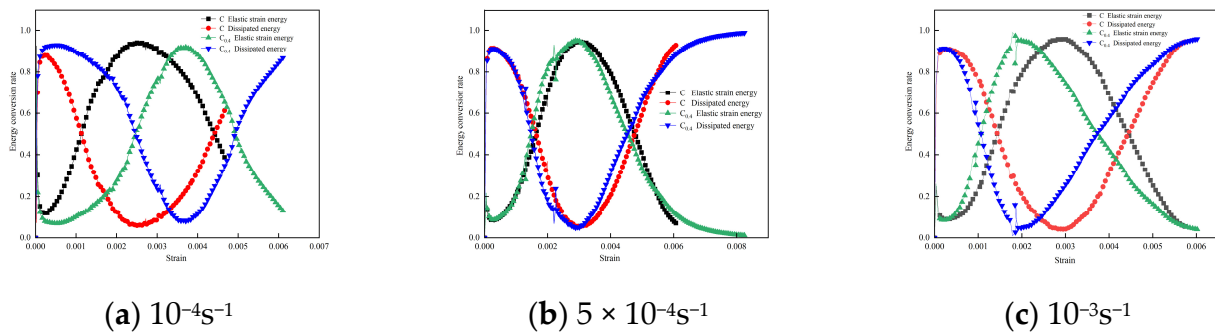


Figure 10. Relationship between energy conversion and stress–strain.



(a) 10^{-4}s^{-1}

(b) $5 \times 10^{-4}\text{s}^{-1}$

(c) 10^{-3}s^{-1}

Figure 11. Energy conversion–strain curves at different strain rates.

- (1) Compression stage (I). Due to the presence of pores and microcracks in the carbon fiber concrete specimen, at this stage, the energy absorbed from the outside of the concrete specimen is essentially used to close the internal pores and microcracks of the specimen, and there is almost no input energy at this time that the elastic strain energy is converted. It can be seen from Figure 10 that the conversion rate of the elastic deformation energy gradually increases and the conversion rate of the dissipation energy gradually decreases during the densification phase.
- (2) Elastic deformation stage (II). When the elastic deformation energy conversion-rate curve intersects with the dissipation energy conversion-rate curve for the first time, i.e., $\alpha = \beta$, the specimen enters the phase of elastic deformation. At this stage, the concrete specimen can be regarded as an ideal linear elastic body, and the concrete mainly undergoes reversible elastic deformation. In the elastic deformation phase, the energy conversion rate of elastic deformation gradually increases, and the conversion rate of dissipated energy gradually decreases. Comparing Figure 9a–c, the energy dissipation at the elastic deformation stage can be seen more clearly at a small strain rate. This is because at a low strain rate, the load is applied over a longer period of time, and crack sliding occurs within the specimen.
- (3) Plastic deformation stage (III). With increasing strain, the energy conversion rate of elastic strain reaches the maximum value, and the conversion rate of the dissipation energy reaches the minimum value. At this point, the specimen enters the plastic deformation phase. At this stage, the concrete specimen gradually loses elasticity under the action of axial tension. The microcracks inside the specimen expand rapidly, the elastic strain energy conversion rate decreases rapidly, and the dissipative energy conversion rate increases sharply. The specimen gradually reaches the limit of its load-bearing capacity and plastic deformation occurs. As can be seen from Figure 9, with the increasing strain rate of the 0.4% carbon fiber concrete specimen, the strain corresponding to the sudden turning point of the dissipated energy is larger than that of the plain concrete. This is because the carbon fiber consumes the deformation energy through its own compression deformation before the dissipation energy reaches the abrupt inflection point, so as to retard the deformation of the specimen. When the

strain rate is small, the energy dissipation phenomenon is serious. As the strain rate increases, the proportion of dissipated energy gradually decreases.

- (4) Destruction stage (IV). With the gradual increase in the axial load, the specimen reaches the peak stress and begins to damage. Numerous cracks appear on the surface of the specimen, and the input strain energy is mainly dissipated in the form of the surface energy and kinetic energy of the cracks. During the destruction phase of the specimen, as α continues to decrease and β gradually increases, a second point occurs where $\alpha = \beta$ occurs and the critical point of permanent concrete damage is reached. After that, the energy conversion rate of the elastic strain continues to decrease and the dissipation energy conversion rate continues to increase, $\alpha < \beta$; the level of elastic strain energy is low; and the specimen is unable to store the elastic strain energy, causing damage to occur.

From Figure 11a–c, it can be seen that the energy conversion rate–strain curves of the plain concrete and 0.4% CFRC have the same trend at different strain rates, but the difference between the curves is due to the influence of the strain rate, and the carbon fiber installation is not negligible. As can be seen from Figure 11, CFRC energy conversion has a significant influence on the strain rate. As the strain rate increases, the maximum value of the elastic strain energy conversion rate increases, and the minimum value of the dissipative energy conversion rate decreases. With the increase in the strain rate, the elastic strain energy fraction of the concrete in the plain concrete is less than the 0.4% CFRC, but the elastic strain energy fraction of the plain concrete is larger than that of the 0.4% CFRC. It shows that the carbon fiber incorporated into concrete can accumulate energy and slow down the energy distribution of the concrete. At higher strain rates, the strain value corresponding to the second $\alpha = \beta$ point of the energy conversion rate–strain curve of the CFRC specimen is larger than that of the plain concrete. It shows that carbon fibers have a significant impact on retarding concrete damage at higher strain rates. At a lower strain rate, the 0.4% CFRC enters the elastic deformation phase first before the plain concrete. This is because the carbon fiber fills the internal pores of the concrete, causing the concrete specimen to complete the compaction phase more quickly.

5. Ontological Modeling Based on Energy Dissipation

5.1. Establishment of the Ontological Model

Damage mechanics suggest that the main mechanism of material degradation is the reduction in the effective area due to microdefects. Let the initial damage degree of the CFRC be 0; the cross-sectional area be A ; and the effective area after damage be A^* , i.e., the physical meaning of the degree of continuity ψ is the ratio of the effective load-bearing cross-sectional area to the cross-sectional area in the initial state:

$$\psi = \frac{A^*}{A} \quad (5)$$

In the formula, if $\psi = 1$, it means the ideal material without defects, and if $\psi = 0$, it means the material state of complete destruction and the loss of the bearing capacity.

For concrete materials, it is common to introduce the damage variable D [27] to describe the degree of damage, i.e.:

$$D = 1 - \psi = 1 - \frac{A^*}{A} \quad (6)$$

The theory of damage mechanics results in the following relationship between nominal and effective stresses in concrete materials:

$$\sigma = \frac{A^*}{A} \sigma^* \quad (7)$$

where σ is nominal stress and σ^* is effective stress.

From Equations (6) and (7), we obtain:

$$\sigma = (1 - D)\sigma^* \tag{8}$$

According to the strain equivalence hypothesis proposed by J. Lemaitre [28], the strain induced by the effective stress acting on the damaged material is the same as the strain induced by the nominal stress acting on the undamaged material, which can be obtained as

$$\sigma = (1 - D)E\varepsilon \tag{9}$$

where E is the elastic modulus and ε is the strain.

5.2. Calculation of Damage Sizes

Approaching the interior of concrete as an innumerable composition of microelements, the degree of damage can be expressed by the ratio of the value of microelements destroyed by damage, N , to the value of microelements destroyed by damage, M , and the value of damage-destroyed microelements is related to the energy dissipation during the damage process. Since the two-parameter WEIBULL probability distribution has been applied to the analysis of concrete volume rupture and failure data, this article assumes that the dissipation energy of CFRC follows the two-parameter WEIBULL probability density function [29]:

$$f(U^d) = \frac{\beta}{\alpha} \left(\frac{U^d}{\alpha}\right)^{\beta-1} \exp\left[-\left(\frac{U^d}{\alpha}\right)^\beta\right] \tag{10}$$

where U^d is the dissipated energy, α is the scale parameter, and β is the shape parameter.

$$N = M \int_0^{U^d} f(x)dx = M \left\{ 1 - \exp\left[-\left(\frac{U^d}{\alpha}\right)^\beta\right] \right\} \tag{11}$$

So, the damage variable D can be expressed as:

$$D = \frac{N}{M} = 1 - \exp\left[-\left(\frac{U^d}{\alpha}\right)^\beta\right] \tag{12}$$

According to Formulas (9) and (12), the constitutive relationship of the uniaxial compression of CFRC based on energy dissipation is as follows:

$$\sigma = E\varepsilon \exp\left[-\left(\frac{U^d}{\alpha}\right)^\beta\right] \tag{13}$$

5.3. Determination of Parameters

α and β are derived in the formula, and two logarithms on both sides of the formula can be obtained at the same time:

$$\ln\left[-\ln\left(\frac{\sigma}{E\varepsilon}\right)\right] = \beta \ln\left(\frac{U^d}{\alpha}\right) \tag{14}$$

In the formula, α and β are obtained by fitting the data obtained from the experiment. Let $x = \ln U^d$, $y = \ln\left[-\ln\left(\frac{\sigma}{E\varepsilon}\right)\right]$, $b = -\beta \ln \alpha$; that is, Equation (14) can be expressed as a linear form of $y = \beta x + b$, so this article uses the linear fitting method to estimate both parameters. The slope obtained is the shape parameter β , and then the scale parameter α can be obtained by $b = -\beta \ln \alpha$. The parameters of the uniaxial compression damaged model of CFRC with different carbon fiber contents are listed in Table 5.

Table 5. Parameters of the damaged model.

Carbon Fiber Content/%	α	β	R^2
0	0.1356	2.36205	0.94
0.2	0.12427	2.48615	0.92
0.4	0.14445	2.62611	0.91
0.6	0.11683	1.77243	0.90
0.8	0.13127	1.19205	0.97

5.4. Model Confirmation

From the α and β values obtained in Table 5 and the stresses, strains, and elastic moduli obtained from the tests, the stress–strain curve of the CFRC damaged model can be calculated and compared with the test curve, as shown in Figure 12.

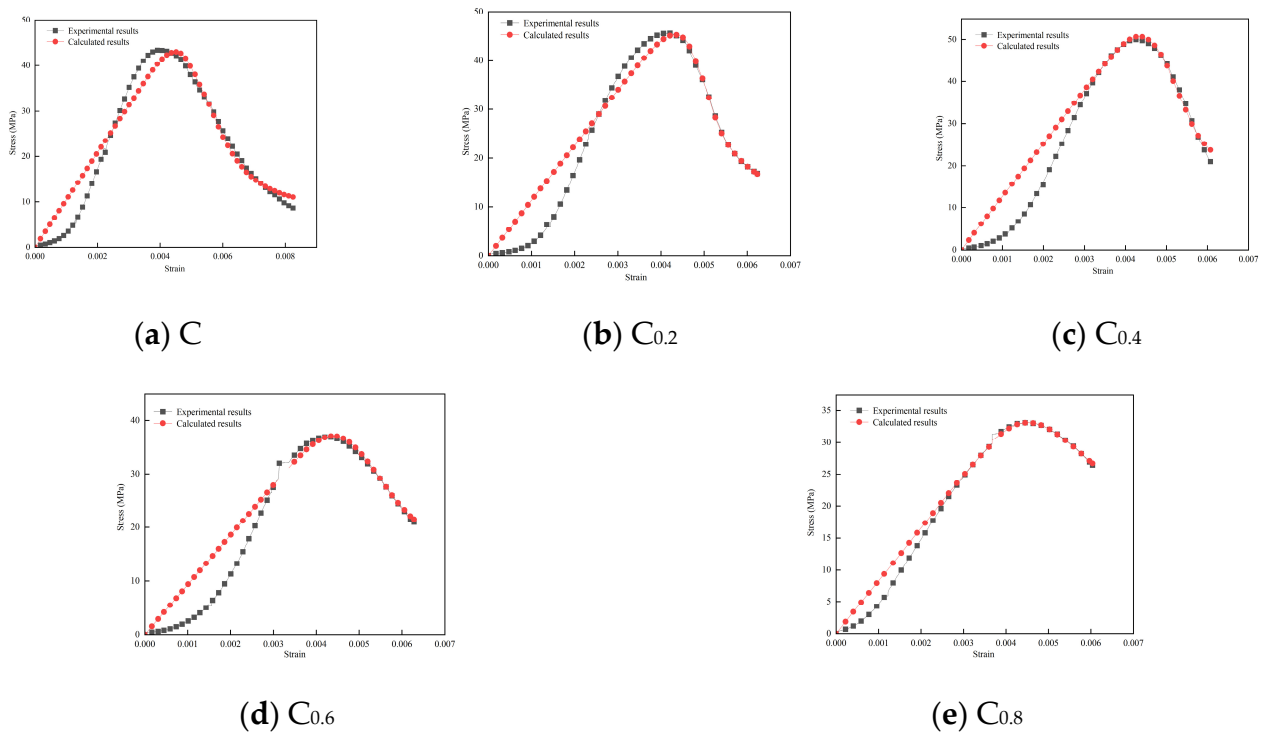


Figure 12. Comparison of stress–strain curve and test curve of CFRC constitutive model.

As can be seen from Figure 12, the calculated curves of the model fit well with the CFRC stress–strain test curves, and the calculated results of the model are higher than the test results in the elastic phase only. This is due to improper testing methods for the elastic deformation and gap compaction phases of the press during the actual test. In general, the energy-dissipation-based uniaxial compression damaged model can better represent the stress–strain relationship of CFRC.

5.5. Damage Development

The damage variable D of CFRC under different carbon fiber contents can be obtained by Formula (12), and the damage evolution law of CFRC is shown in Figure 13. It can be seen from the figure that when the ultimate elongation of the CFRC specimen is reached, with the increase in carbon fiber doping, the degree of damage decreases, and it can be found that the carbon fiber can effectively limit the damage development of CFRC and delay the deformation of the specimen.

In the process of uniaxial compression, the change trend of the damage variable D shows “S” type growth. The first gentle stage is the elastic stage of the CFRC specimen. At

this point, the specimen can be regarded as an ideal linear elastic body, and the damage development is slow. After the transition from the flat stage to the rising stage, the conversion rate of the dissipated energy increases sharply due to the increasing friction between the fiber and the concrete matrix, and the specimen is in the stage of plastic deformation. After reaching the peak tension, the curvature of the specimen begins to transition from steep to gentle. This is because the bridging effect of the fiber can effectively inhibit the formation of the cracks, and the loss energy conversion rate of the CFRC specimen is reduced. At this point, the specimen is in the failure stage.

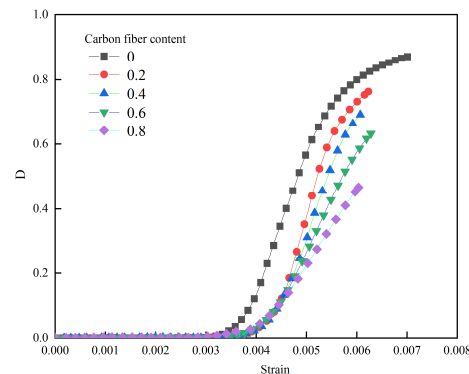


Figure 13. Damage evolution of CFRC.

6. Conclusions

In this paper, CFRC with five kinds of fiber content was prepared for a uniaxial compression test. The effects of carbon fiber contents and strain rate on the mechanical properties of CFRC were studied. Combined with the failure mode, the damage model of CFRC is established based on the principle of energy conversion. Although this paper proposes to calculate the damage model of concrete specimens by the dissipation energy of concrete specimens, it has certain limitations. The next work is to determine whether the model is suitable for other fiber-reinforced concrete or building materials and the engineering application of the model. The conclusions are as follows:

- (1) When the mixing amount of carbon fiber is 0.4%, the overall performance of the carbon fiber concrete is optimal. The compressive strength of the specimen is 15.02% higher than that of the reference concrete, the splitting tensile strength is increased by 51.12%, and the total strain energy and elastic strain energy reach their peak. With the gradual increase in the carbon fiber dosage, each energy of the carbon fiber concrete specimens at the peak stress showed a trend of increasing and then decreasing, and the peak strain gradually increased. At different strain rates, the compressive strength of the optimal content group is 10.01%, 15.02%, and 18.27% higher than that of the plain concrete.
- (2) The energy dissipation of the plain concrete at low strain rates is important in the compaction-density phase of the deformation damage process in CFRC; in the elastic deformation phase, the input energy is mainly converted into elastic strain energy storage, and the elastic strain energy ratio increases significantly with the increase in the strain rate. In the plastic deformation stage, the larger the strain rate. At the smaller proportion of dissipated energy and the same strain rate of the carbon fiber concrete, the dissipation energy increases significantly at the same strain rate as the plain concrete, effectively retarding the specimen deformation.
- (3) As the strain rate increases, the peak value increases, followed by a decrease in the minimum value of b , indicating that the strain rate has a large influence on the energy distribution. As the strain rate increases, the elastic strain energy percentage of the base concrete increases more than that of carbon fiber concrete, but the elastic strain energy percentage of carbon fibers is still higher than that of plain concrete, indicating

that the carbon fibers have the ability to accumulate elastic strain energy and slow down the energy distribution of the concrete.

- (4) The CFRC material model is based on the damage mechanics theory and the probabilistic statistical method, and the calculated curve of the model fits well with the CFRC stress–strain test curve, which reflects the effect of carbon fiber doping on the CFRC material damage.

Author Contributions: Conceptualization, R.Z.; methodology, J.P.; software, J.S. and R.Z.; validation, R.Z., J.S., Y.S. and G.X.; formal analysis, R.Z.; investigation, R.Z.; resources, J.P.; data curation, J.S.; writing—original draft preparation, R.Z.; writing—review and editing, R.Z.; visualization, J.S.; supervision, J.P. All authors have read and agreed to the published version of the manuscript.

Funding: Funding was received by the University Natural Science Research Project of Anhui Province (2023AH051219).

Data Availability Statement: All data used to support the findings of this study are available from the corresponding author upon request.

Conflicts of Interest: The authors have no relevant financial or non-financial interests to disclose.

References

- Pontinha, A.D.R.; Mäntyneva, J.; Santos, P.; Durães, L. Thermomechanical Performance Assessment of Sustainable Buildings' Insulating Materials under Accelerated Ageing Conditions. *Gels* **2023**, *9*, 241. [\[CrossRef\]](#)
- Mo, L.; Deng, M.; Tang, M.; Al-Tabbaa, A. MgO expansive cement and concrete in China: Past, present and future. *Cem. Concr. Res.* **2014**, *57*, 1–12. [\[CrossRef\]](#)
- Lawler, J.S.; Wilhelm, T.; Zampini, D.; Shah, S.P. Fracture processes of hybrid fiber-reinforced mortar. *Mater. Struct.* **2003**, *36*, 197–208. [\[CrossRef\]](#)
- Beeldens, A.; Van Gemert, D.; Schorn, H.; Ohama, Y.; Czarnecki, L. From microstructure to macrostructure: An integrated model of structure formation in polymer-modified concrete. *Mater. Struct.* **2005**, *38*, 601–607. [\[CrossRef\]](#)
- Aydin, A.C. Self compactability of high volume hybrid fiber reinforced concrete. *Constr. Build. Mater.* **2007**, *21*, 1149–1154. [\[CrossRef\]](#)
- Guo, H.; Tao, J.; Chen, Y.; Li, D.; Jia, B.; Zhai, Y. Effect of steel and polypropylene fibers on the quasi-static and dynamic splitting tensile properties of high-strength concrete. *Constr. Build. Mater.* **2019**, *224*, 504–514. [\[CrossRef\]](#)
- Zheng, Y.; Zhang, Y.; Zhuo, J.; Zhang, Y.; Wan, C. A review of the mechanical properties and durability of basalt fiber-reinforced concrete. *Constr. Build. Mater.* **2022**, *359*, 129360. [\[CrossRef\]](#)
- Song, P.S.; Hwang, S. Mechanical properties of high-strength steel fiber-reinforced concrete. *Constr. Build. Mater.* **2004**, *18*, 669–673. [\[CrossRef\]](#)
- Muthukumarana, T.V.; Arachchi MA VH, M.; Somarathna HM, C.C.; Raman, S.N. A review on the variation of mechanical properties of carbon fiber-reinforced concrete. *Constr. Build. Mater.* **2023**, *366*, 130173. [\[CrossRef\]](#)
- Chen, T.; Wang, Z.H.; Wang, A.; Bai, E.; Zhu, X. Comparative study on the static and dynamic mechanical properties and micro-mechanism of carbon fiber and carbon nanofiber reinforced concrete. *Case Stud. Constr. Mater.* **2023**, *18*, e01827. [\[CrossRef\]](#)
- Patchen, A.; Young, S.; Penumadu, D. An Investigation of Mechanical Properties of Recycled Carbon Fiber Reinforced Ultra-High-Performance Concrete. *Materials* **2022**, *16*, 314. [\[CrossRef\]](#)
- Wu, L.; Lu, Z.; Zhuang, C.; Chen, Y.; Hu, R. Mechanical properties of nano SiO₂ and carbon fiber reinforced concrete after exposure to high temperatures. *Materials* **2019**, *12*, 3773. [\[CrossRef\]](#)
- Boris, R.; Antonovich, V.; Spudulis, Ē.; Volochko, A.; Stonis, R. Effect of carbon fiber on medium-cement heat-resistant concrete properties. *Refract. Ind. Ceram.* **2014**, *55*, 352–355. [\[CrossRef\]](#)
- Kizilkanat, A.B. Experimental evaluation of mechanical properties and fracture behavior of carbon fiber reinforced high strength concrete. *Period. Polytech. Civ. Eng.* **2016**, *60*, 289–296. [\[CrossRef\]](#)
- Kan, W.; Yang, Z.; Yu, L. Study on Frost Resistance of the Carbon-Fiber-Reinforced Concrete. *Appl. Sci.* **2022**, *12*, 3823. [\[CrossRef\]](#)
- Deng, Z.H.; Zhou, Y.W.; Jiang, J.S.; Huang, X.; Liu, B. Mechanical properties and uniaxial constitutive model of fiber-reinforced coral aggregate concrete. *Struct. Concr.* **2023**, *24*, 4259–4275. [\[CrossRef\]](#)
- Wang, H.; Dang, F.; Ren, J.; Li, Y.; Zhu, L. Experimental Research on the Energy Evolution of Concrete under Impact Loading. *Materials* **2023**, *16*, 5140. [\[CrossRef\]](#)
- Geng, K.; Chai, J.; Qin, Y.; Li, X.; Duan, M.; Liang, D. Exploring the brittleness and fractal characteristics of basalt fiber reinforced concrete under impact load based on the principle of energy dissipation. *Mater. Struct.* **2022**, *55*, 78. [\[CrossRef\]](#)
- Ren, J.; Dang, F.; Wang, H.; Xue, Y.; Fang, J. Enhancement mechanism of the dynamic strength of concrete based on the energy principle. *Materials* **2018**, *11*, 1274. [\[CrossRef\]](#)
- Li, Y.; Zhai, Y.; Liu, X.; Liang, W. Research on fractal characteristics and energy dissipation of concrete suffered freeze-thaw cycle action and impact loading. *Materials* **2019**, *12*, 2585. [\[CrossRef\]](#)

21. GB/T50081-2002; Standard for Test Method of Mechanical Properties on Ordinary Concrete. China Architecture and Building Press: Beijing, China, 2003. (In Chinese)
22. Zhao, Z.; Ma, W.; Fu, X.; Yuan, J. Energy theory and application of rocks. *Arab. J. Geosci.* **2019**, *12*, 1–26. [[CrossRef](#)]
23. Wang, C.; He, B.; Hou, X.; Li, J.; Liu, L. Stress–energy mechanism for rock failure evolution based on damage mechanics in hard rock. *Rock Mech. Rock Eng.* **2020**, *53*, 1021–1037. [[CrossRef](#)]
24. Meng, Q.; Zhang, M.; Han, L.; Pu, H.; Nie, T. Effects of acoustic emission and energy evolution of rock specimens under the uniaxial cyclic loading and unloading compression. *Rock Mech. Rock Eng.* **2016**, *49*, 3873–3886. [[CrossRef](#)]
25. Jin, X.C.; Hou, C.; Fan, X.L.; Lu, C.; Yang, H.; Shu, X.; Wang, Z. Quasi-static and dynamic experimental studies on the tensile strength and failure pattern of concrete and mortar discs. *Sci. Rep.* **2017**, *7*, 15305. [[CrossRef](#)] [[PubMed](#)]
26. Chen, X.; Ge, L.; Zhou, J.; Wu, S. Dynamic Brazilian test of concrete using split Hopkinson pressure bar. *Mater. Struct.* **2017**, *50*, 1–15. [[CrossRef](#)]
27. Xiao, Y.J.; Chen, Z.S.; Zhou, J.T.; Leng, Y.; Xia, R. Concrete plastic-damage factor for finite element analysis: Concept, simulation, and experiment. *Adv. Mech. Eng.* **2017**, *9*, 1687814017719642. [[CrossRef](#)]
28. Lemaitre, J. A Continuous Damage Mechanics Model for Ductile Fracture. *J. Eng. Mater. Technol.* **1985**, *107*, 83–89. [[CrossRef](#)]
29. Wang, C.; Fu, P.; Liu, Z.; Xu, Z.; Wen, T.; Zhu, Y.; Long, Y.; Jiang, J. Study of the Durability Damage of Ultrahigh Toughness Fiber Concrete Based on Grayscale Prediction and the Weibull Model. *Buildings* **2022**, *12*, 746. [[CrossRef](#)]

Disclaimer/Publisher’s Note: The statements, opinions and data contained in all publications are solely those of the individual author(s) and contributor(s) and not of MDPI and/or the editor(s). MDPI and/or the editor(s) disclaim responsibility for any injury to people or property resulting from any ideas, methods, instructions or products referred to in the content.